J|A|C|S
ARTICLES
Published on Web 07/28/2006

Chirally Directed Formation of Nanometer-Scale Proline Clusters

Sunnie Myung, Marco Fioroni, Ryan R. Julian,† Stormy L. Koeniger, Mu-Hyun Baik,* and David E. Clemmer*

Contribution from the Department of Chemistry and School of Informatics, Indiana University, Bloomington, Indiana 47405

Received April 6, 2006; E-mail: mbaik@indiana.edu; clemmer@indiana.edu.

Abstract: Ion mobility measurements, combined with molecular mechanics simulations, are used to study enantiopure and racemic proline clusters formed by electrospray ionization. Broad distributions of cluster sizes and charge states are observed, ranging from clusters containing only a few proline units to clusters that contain more than 100 proline units (i.e., protonated clusters of the form $[x\text{Pro} + n\text{H}]^{n+}$ with $x = 1$ to >100 and $n = 1-7$). As the sizes of clusters increase, there is direct evidence for nanometer scale, chirally induced organization into specific structures. For $n = 4$ and 5, enantiopure clusters of ~50 to 100 prolines assemble into structures that are more elongated than the most compact structure that is observed from the racemic proline clusters. A molecular analogue, *cis*-4-hydroxy-proline, displays significantly different behavior, indicating that in addition to the rigidity of the side chain ring, intermolecular interactions are important in the formation of chirally directed clusters. This is the first case in which assemblies of chirally selective elongated structures are observed in this size range of amino acid clusters. Relationships between enantiopurity, cluster shape, and overall energetics are discussed.

Introduction

Spontaneous chiral resolution was first reported in 1848, when Pasteur mechanically separated two enantiomeric forms of sodium ammonium tartrate tetrahydrate from a racemic mixture.[1] Since then, few examples of spontaneous resolution have been reported.[2] An understanding of how chirality influences the formation of crystals remains elusive.[3,4] Although many factors may play a role, molecular structure and noncovalent intermolecular interactions must ultimately exert some control over the crystal formation process.[3,5] To better understand fundamental aspects of resolution, it is important to study the influence of chirality on the organization of molecular clusters, an intermediate size regime, between atomic and bulk states.[6−18] With the advent of electrospray ionization (ESI),[19] it is possible to produce and examine clusters of biologically important molecules.[14−18,20−29] One of the most studied systems is serine octamer,[20−29] which forms as a stable magic cluster that displays an unusual homochiral preference, despite the fact that serine does not undergo spontaneous chiral resolution upon bulk crystallization.[30] Unlike the octamer, the serine decamer displays a heterochiral preference, and still larger clusters (>20 monomer

† Present address: University of California Riverside, Riverside, CA 92521.

(1) Pasteur, L. *Ann. Phys.*, **1848**, *24*, 442.
(2) Jacques, J.; Collet, A.; Wilen, S. H. *Enantiomers, Racemates, and Resolutions*. John Wiley & Sons: New York, 1981 (reprint edition 1991, reissued with corrections, Krieger Publishing Company, Malabar, FL, 1994).
(3) Pérez-García, L.; Amabilino, D. B. *Chem. Soc. Rev.* **2002**, *31*, 342.
(4) Custelcean, R.; Gorbunova, M. G. *Cryst. Eng. Comm.* **2005**, *7*, 297.
(5) Li, A. J.; Ojala, W. H.; Grant, D. J. W. *J. Pharm. Sci.* **2001**, *90*, 1523.
(6) Kroto, H. W.; Heath, J. R.; O′Brien, S. C.; Curl, R. F.; Smalley, R. E. *Nature* **1985**, *318*, 162.
(7) Clemmer, D. E.; Shelimov, K. B.; Jarrold, M. F. *Nature* **1994,** *367*, 718. Clemmer, D. E.; Hunter, J. M.; Shelimov, K. B.; Jarrold, M. F. *Nature* **1994**, *372*, 248. Clemmer, D. E.; Shelimov, K. B.; Jarrold, M. F. *J. Am. Chem. Soc.* **1994**, *116*, 5971. Shvartsburg, A. A.; Liu, B.; Lu, Z.-Y.; Wang, C. Z.; Jarrold, M. F.; Ho, K.-M. *Phys. Rev. Lett.* **1999**, *83*, 2167. Ho, K.-M.; Shvartsburg, A. A.; Pan, B. C.; Lu, Z. Y.; Wang, C. Z.; Wacker, J. G.; Fye, J. L.; Jarrold, M. F. *Nature* **1998**, *392*, 582.
(8) Speranza, M. In *Advances in Physical Organic Chemistry*; Richard, J. P. Ed.; Elsevier: London, **2004**; p147.
(9) Smirnov, B. M. *Clusters and Small Particles: In Gases and Plasmas*; Springer: New York, **2000**.
(10) Baèiæ, Z.; Miller, R. E. *J. Phys. Chem.* **1996**, *100*, 12945.
(11) Castleman, A. W. Jr.; Bowen, K. H. Jr. *J. Phys. Chem.* **1996**, *100*, 12911.
(12) Rusyniak, M. J.; Ibrahim, Y. M.; Wright, D. L.; Khanna, S. N.; El-Shall, M. S. *J. Am. Chem. Soc.* **2003**, *125*, 12001.
(13) Kebarle, P. *Annu. Rev. Phys. Chem.* **1977**, *28*, 445.
(14) Desfrancois, C.; Carles, S.; Schermann, J. P. *Chem. Rev.* **2000**, *100*, 3943.
(15) Stace, A. *Science* **2001**, *294*, 1292.
(16) Hammond, R. B.; Pencheva, K.; Roberts, K. J. *J. Phys. Chem. B* **2005**, 109, 19550.
(17) Borman, S. *Chem. Eng. News* **2004**, *82* (20), 42.
(18) Shin, J.-W.; Hammer, N. I.; Diken, E. G.; Johnson, M. A.; Walters, R. S.; Jaeger, T. D.; Duncan, M. A.; Christie, R. A.; Jordan, K. D. *Science* **2004**, *304*, 1137.
(19) Fenn, J. B.; Mann, M.; Meng, C. K.; Wong, S. F. Whitehouse, C. M. *Science* **1989**, *246*, 64.
(20) Cooks, G. R.; Zhang, D.; Koch, K. J.; Gozzo, F. C.; Eberlin, M. N. *Anal. Chem.* **2001**, *73*, 3646.
(21) Julian, R. R.; Hodyss, R.; Kinnear, B.; Jarrold, M. F.; Beauchamp, J. L. *J. Phys. Chem. B* **2002**, *106*, 1219.
(22) Counterman, A. E.; Clemmer, D. E. *J. Phys. Chem. B* **2001**, 105, 8092.
(23) Koch, K. J.; Gozzo, F. C.; Zhang, D.; Eberlin, M. N.; Cooks, G. R. *Chem. Commun.* **2001**, 1854.
(24) Takáts, Z.; Nanita, S. C.; Cooks, R. G. *Angew. Chem., Int. Ed.* **2003**, 42, 3521.
(25) Julian, R. R.; Myung, S.; Clemmer, D. E. *J. Am. Chem. Soc.* **2004**, 126, 4110.
(26) Nemes, P.; Schlosser, G.; Vékey, K.*J. Mass Spectrom.* **2005**, 40, 43.
(27) Mazurek, U.; Engeser, M.; Lifshitz, C. *Int. J. Mass Spectrom.* **2006**, 249, 473.
(28) Schalley, C. A.; Weis, P. *Int. J. Mass Spectrom.* **2002**, 221, 9.
(29) Myung, S.; Julian, R. R.; Nantia, S. C.; Cooks, R. G.; Clemmer, D. E. *J. Phys. Chem. B* **2004**, *108*, 6105.
(30) Kistenmacher, T. J.; Rand, G. A.; Marsh, R. E. *Acta Crystallogr.* **1974**, B30, 2573.

units) apparently show no evidence for chiral preference.[25] Additional considerations suggest that overall, the organization of structure decreases for clusters containing ~20−70 serine monomer units,[25,29] suggesting that the influence of chirality on structure in clusters of serine is a local phenomenon (i.e., on the molecular scale).

In this work, we examine the influence of monomer chirality in the formation of proline and *cis*-4-hydroxy-proline clusters. Proline (**1**) is the only naturally occurring amino acid that contains a cyclic side chain with a secondary amine and is often important in establishing structure and influencing function in peptides and proteins.[31−35] *cis*-4-Hydroxy-proline (**2**) has a similar structure, with an additional hydroxyl group associated with the pyrrolidine ring.

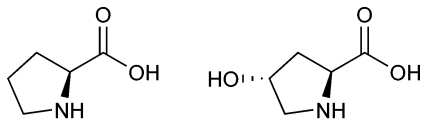

1 **2**

Here, we report that proline assemblies show evidence for chiral preference on the nanometer scale (i.e., clusters containing between ~50 to 100 monomer units). We explore the relationship of monomer structure and chirality, cluster size, and intermolecular interactions by simulations that utilize specifically customized force fields in a molecular mechanics framework. The combination of experiment and theory provides a consistent picture of chiral resolution at the nanometer scale and provides insight about how structure arises from finely balanced forces that govern assembly.

Experimental Section

Overview. Ion mobility spectrometry (IMS) techniques have been described in detail previously.[36−39] Only a brief description of the experiment is presented here. Charged droplets are produced by ESI and enter a differentially pumped source region (~2 Torr) where solvent evaporation occurs. A continuous beam of protonated amino acid clusters is focused into an hourglass ion funnel[40,41] and accumulated for ~15 ms. Experiments are initiated by gating concentrated packets of ions (using a 100 μs pulse) from the ion funnel into the drift tube, similar to approaches described by others.[39,41,42] The drift tube is filled with ~3.3 Torr of He buffer gas (300 K), and ions are separated under the influence of a weak uniform electric field (12 V·cm^{-1}). The drift tube also incorporates an ion funnel at the exit region that is used to focus ions through the exit aperture.[39,43] Under the conditions employed, collisional excitation of the ions throughout the instrument is minimal. Upon exiting the drift tube, ions enter the source region of a reflectron geometry time-of-flight mass spectrometer (MS). Flight times, in the evacuated flight tube, are shorter (μs time scales) than drift times (ms time scales) associated with the ion mobility separation, allowing drift and flight times to be recorded using a nested approach.[44−46]

Sample Preparation. The L- and D-proline and *cis*-4-hydroxy-proline (Fluka, 99% purity) were used without further purification. All solutions were prepared in 49:49:2 water/acetonitrile/acetic acid at a total concentration of 0.01 M. Solutions were electrosprayed using a flow rate of 1.3 μL·min^{-1}.

Determining Experimental Collision Cross Sections from Mobility Measurements. The mobility of an ion through a buffer gas depends on its charge state and average collision cross section. High-charge state ions usually have higher mobilities (for a given m/z) than low-charge state ions because they experience a greater drift force. The collision cross section depends on the ion structure.[29,37,38,47−49] Compact geometries will have higher mobilities (shorter drift times) than more elongated structures. Collision cross sections (Ω) are determined from experimental measurements using the relation[49]

$$\Omega = \frac{(18\pi)^{1/2}}{16}\frac{ze}{(k_bT)^{1/2}}\left[\frac{1}{m_I}+\frac{1}{m_B}\right]^{1/2}\frac{t_DE}{L}\frac{760}{P}\frac{T}{273.2}\frac{1}{N}$$

where e, z, m_I, and m_B correspond to the electron charge, charge state, and masses of the ion and buffer gas, respectively. N and k_b are the neutral number density (at 273.2 K and 760 Torr) and Boltzmann's constant, respectively. The electric field strength (E), drift tube length (L), buffer gas pressure (P in Torr), and buffer gas temperature (T in Kelvin) are precisely controlled.

The total arrival time is a composite of the time that ions spend in the drift tube, exit ion funnel, and mass spectrometer. It is necessary to account for these times to determine the time spent in the drift region. This is done by calibration to ions with known cross sections under varying sets of conditions. After calibration, cross section measurements

(31) Schwartz, T. W. *FEBS Lett.* **1986**, 200, 1.
(32) Bhattacharyya, R.; Chakrabarti, P. *J. Mol. Biol.* **2003**, 331, 925. Williams, K. A.; Deber, C. M. *Biochemistry* **1991**, *30*, 8919. Woolfson, D. N.; Mortishiresmith, R. J.; Williams, D. H. *Biochem. Biophys. Res. Commun.* **1991**, 175, 733.
(33) Chou, P. Y.; Fasman, G. D. *J. Mol. Biol.* **1977**, 115, 135.
(34) Rose, G. D.; Gierasch, L. M.; Smith, J. A.*Adv. Protein Chem.* **1985**, 37, 1.
(35) Garrett, R. H.; Grisham, C. M. *Biochemistry*; Harcourt College Publishers: Orlando, **1999**; p 174.
(36) Ion mobility spectrometry methods are discussed in the following references: Hagen, D. F. *Anal. Chem.* **1979**, *51*, 870. Tou, J. C.; Boggs, G. U. *Anal. Chem.* **1976**, *48*, 1351. Karpas, Z.; Cohen, M. J.; Stimac, R. M.; Wernlund, R. F. *Int. J. Mass Spectrom. Ion Processes* **1986**, 74, 153. Hill, H. H.; Siems, W. F.; St. Louis, R. H.; McMinn, D. G. *Anal. Chem.* **1990**, *62*, 2, A1201. St. Louis, R. H.; Hill, H. H. *Cr. Rev. Anal. Chem.* **1990**, *21*, 321. Jarrold, M. F. *J. Phys. Chem.* **1995**, *99*, 11. Hoaglund-Hyzer, C. S.; Lee, Y. J.; Counterman, A. E.; Clemmer, D. E. *Anal. Chem.* **2002**, *74*, 992. Wyttenbach, T.; Bowers, M. T. *Top. Curr. Chem.* **2003**, 225, 207. Creaser, C. S.; Griffiths, J. R.; Bramwell, C. J.; Noreen, S.; Hill, C. A.; Thomas, C. L. P. *Analyst* **2004**, 129, 984. McLean, J. A.; Ruotolo, B. T.; Gillig, K. J. Russell, D. H. *Int. J. Mass Spectrom.* **2005**, 240, 301.
(37) Clemmer, D. E.; Jarrold, M. F. *J. Mass Spectrom.* **1997**, 32, 577.
(38) von Helden, G.; Hsu, M. T.; Kemper, P. R.; Bowers, M. T.*J. Chem. Phys.* **1991**, 95, 3835.
(39) Tang, K.; Shvartsburg, A. A.; Lee, H.; Prior, D. C.; Buschbach, M. A.; Li, F.; Tomachev, A.; Anderson, G. A.; Smith, R. D. *Anal. Chem.* **2005**, 77, 3330.
(40) Shaffer, S. A.; Tang, K. Q.; Anderson, G. A.; Prior, D. C.; Udseth, H. R.; Smith, R. D. *Rapid Commun. Mass Spectrom.* **1997**, 11, 1813. Shaffer, S. A.; Prior, D. C.; Anderson, G. A.; Udseth, H. R.; Smith, R. D. *Anal. Chem.* **1998**, 70, 4111. Shaffer, S. A.; Tolmachev, A.; Prior, D. C.; Anderson, G. A.; Udseth, H. R.; Smith, R. D. *Anal. Chem.* **1999**, *71*, 2957. Kim, T.; Tolmachev, A. V.; Harkewicz, R.; Prior, D. C.; Anderson, G.; Udseth, H. R.; Smith R. D. Bailey, T. H.; Rakov, S.; Futrell, J. H. *Anal. Chem.* **2000**, 72, 2247.
(41) Wyttenbach, T.; Kemper, P. R.; Bowers, M. T. *Int. J. Mass Spectrom.* **2001**, 212, 13.
(42) Hoaglund, C. S.; Valentine, S. J.; Clemmer, D. E. *Anal. Chem.* **1997**, *69*, 4156. Myung, S., et al. *Anal. Chem.* **2003**, *75*, 5137.
(43) Koeniger, S. L.; Merenbloom, S. I.; Valentine, S. J.; Udseth, H.; Smith, R.; Clemmer, D. E. *An IMS−IMS Analogue of MS-MS* (in press Anal. *Chem.*). Koeniger, S. L.; Merenbloom, S. I.; Clemmer, D. E. *J. Phys. Chem. B* **2006,** *110*, 7017. Merenbloom, S. I.; Koeniger, S. L.; Valentine, S. J.; Plasencia, M. D.; Clemmer, D. E. (ASAP article DOI: 10.1021/ac052208e, *Anal. Chem.* **2006**).
(44) Hoaglund, C. S.; Valentine, S. J.; Sporleder, C. R.; Reilly, J. P.; Clemmer, D. E. *Anal. Chem.* **1998**, *70*, 2236. Henderson, S. C.; Valentine, S. J.; Counterman, A. E.; Clemmer, D. E. *Anal. Chem.* **1999**, *71*, 291.
(45) Rutolo, B. T.; McLean, J. A.; Gillig, K. J.; Russell, D. H. *J. Mass Spectrom.* **2004**, 39, 361.
(46) Steiner, W. E.; Clowers, B. H.; Matz, L. M.; Siems, W. F.; Hill, H. H.*Anal. Chem.* **2002**, 74, 4343.
(47) Valentine, S. J.; Counterman, A. E.; Hoaglund, C. S.; Reilly, J. P.; Clemmer, D. E. *J. Am. Soc. Mass Spectrom.* **1998**, *9*, 1213.
(48) Jarrold, M. F.; Constant, V. A. *Phys. Rev. Lett.* **1991**, 67, 2994. Mesleh, M. F.; Hunter, J. M.; Shvartsburg, A. A.; Schatz, G. C.; Jarrold, M. F. *J. Phys. Chem.* **1996**, *100*, 16082. Wyttenbach, T.; von Helden, G.; Bowers, M. T. *J. Am. Chem. Soc.* **1996**, *118*, 8355. Clemmer, D. E.; Hudgins, R. R.; Jarrold, M. F. *J. Am. Chem. Soc.* **1995**, *117*, 10141.
(49) Mason, E. A.; McDaniel, E. W. *Tansport Properties of Ions in Gases* Wiley: New York, New York **1988**. Hirschfelder, J. O.; Curtiss, C. F.; Bird, R. B. *Molecular Theory of Gases and Liquids* Wiley: New York **1954**.

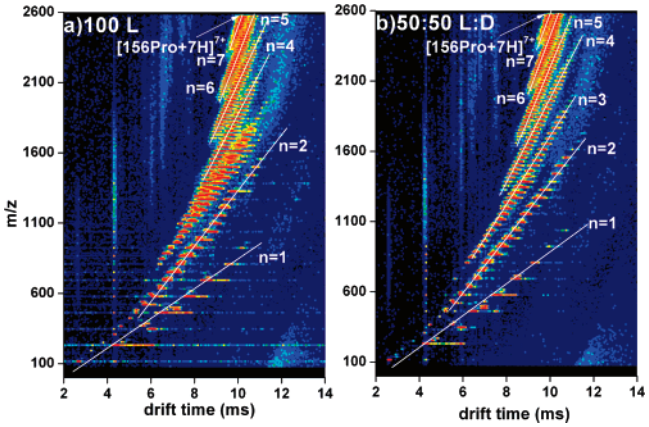

Figure 1. Two-dimensional plot of drift time (ms) versus *m*/*z* ratios for an electrosprayed 0.01 M solution of (a) enantiopure (100:0 L:D) and (b) racemic (50:50 L:D) proline. Different charge-state families are indicated by the white lines and *n*, where *n* represents the charge state. The intensity of different features is shown using a false color scheme in which the least intense features are represented in navy and the most intense features are represented in red.

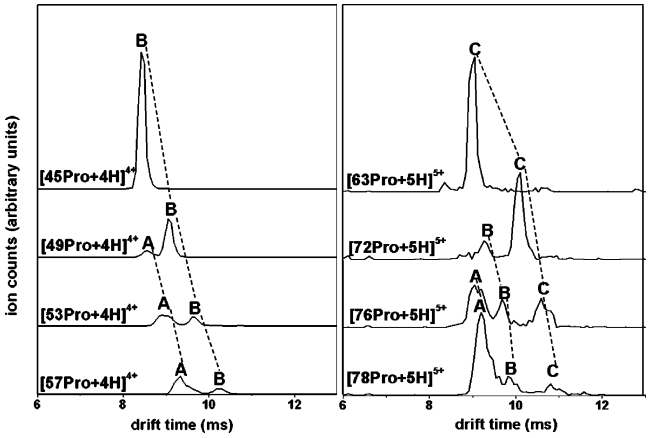

Figure 2. Drift time distributions for enantiopure solution of proline corresponding to $[x\text{Pro} + 4\text{H}]^{4+}$ (x = 45, 49, 53, and 57) and $[x\text{Pro} + 5\text{H}]^{5+}$ (x = 63, 72, 76, and 78) charge-state families. Positions of the maximum peaks are labeled A, B, and C, in the order from the highest to lowest mobility peaks. The diagonal dashed lines are provided to help the reader follow peaks from common mobility families. Clusters in the $n = 4$ charge-state family display two distinguishable peaks whereas the clusters in the $n = 5$ charge-state family show three. Drift-time distributions were obtained by integrating over narrow regions of the drift-time (*m*/*z*) dataset (shown in Figure 1). See text for more detail on the relative abundances of these clusters as a function of cluster size.

are indistinguishable from measurements obtained using other nonfunnel instrument designs.

Computations of Model Geometries for Comparison with Experiment. Because of the large size of the proline clusters studied here, we use molecular mechanics-based modeling techniques[50] to generate trial structures. We began by exploring a series of trial geometries that were generated from the crystal structure of L-proline[51] and LD-proline[52] utilizing the zwitterionic form of proline as the monomeric unit. Cross sections for these unoptimized structures were calculated using the exact hard spheres scattering (EHSS) method.[53] After establishing a rough correlation between the experimental measurements and computationally assumed cluster shapes, we performed more elaborate molecular mechanics simulations using the GROMACS (Version 3.1.2) package.[54−56] Clusters were placed at the center of a cubic box with a width of 16 nm to satisfy the minimum image convention within the periodic boundary condition formalism.[54] Nonbonded interactions were evaluated by using a twin-range cutoff, where the short- and long-range cutoff dimensions were both set to 4.5 nm to include the entire cluster. Minimizations were performed using a conjugate gradient algorithm and were considered converged to a minimum when the absolute value of the gradient was ≤ 1 kJ·mol^{-1}·nm^{-1}. Standard force fields, which are designed for modeling proline in a protein environment or in crystalline form as diblocked peptides, are expected to give poor structures and unreliable energies.[57] Therefore, a new set of bonded and nonbonded force-field parameters for the proline model were developed. Details are reported as Supporting Information.

Results and Discussion

IMS-MS Spectra. Figure 1 shows a typical two-dimensional nested ion mobility mass spectrum obtained upon electrospraying 0.01 M solutions of enantiopure (100:0 L:D) and racemic (50:50 L:D) proline. Peaks fall into families according to their charge state and size, designated here by $[x\text{Pro} + n\text{H}]^{n+}$, where *n* corresponds to the charge state and *x* refers to the number of monomer units in the cluster. In the racemic solution, there are a total of seven charge states that are well separated in the drift-time dimension. For both solutions, the maximum cluster size observed in the drift(flight)-time range that is used for the measurement is $x = 156$. There are striking differences between the enantiopure and racemic cluster data, especially for larger clusters that are unlike any other systems that we have studied.[58] Clusters from enantiopure solutions are separated into $n = 1$, 2, and 4−7 charge states. The $n = 3$ region is not well resolved from $n = 4$, and it contains more than one family of peaks. These are not present in the data for the racemic distribution. Data recorded on different days and several instruments are highly reproducible and indicate that the presence of additional peaks is always associated with the enantiopurity of proline solution.

Ion Mobility Distributions and Collision Cross Sections. To better understand the overlapping features that arise from the enantiopure solution, it is useful to examine ion mobility distribution slices for individual cluster sizes. These distributions are taken for all clusters with unique *m*/*z* values for $n = 4$ and 5 charge-state families. The selection of unique *m*/*z* values ensures that there is no contribution to the ion mobility distribution from other charge states. The distributions of individual cluster sizes are acquired by integrating horizontally across ion intensities in the two-dimensional plot shown in Figure 1 at specific *m*/*z* values. Figure 2 shows the mobility distribution obtained for several enantiopure (L-proline) $[x\text{Pro} + 4\text{H}]^{4+}$ (x = 45, 49, 53, and 57) clusters from the $n =$ 4 family. The distribution for $[45\text{Pro} + 4\text{H}]^{4+}$ shows a single peak (B) arriving at ~8.5 ms. It is particularly interesting that many of the $[x\text{Pro} + 4\text{H}]^{4+}$ sizes exhibit two ion mobility peaks.

(50) Mark E. Tuckerman, Glenn J. Martyna;*J. Phys. Chem. B* **2000**, 104, 159
(51) Kayushina, R. L.; Vainshtein, B. K. *Inst. Cryst. Moscow, Kristallografiya* **1965**, 10, 834.
(52) Myung, S.; Pink, M.; Baik, M.; Clemmer, D. E. *Acta Crystallogr.* **2005**, *C61*, 506.
(53) Shavartsburg, A. A.; Jarrold, M. F. *Chem. Phys. Lett.* **1996**, 261, 86.
(54) van der Spoel, D.; Lindhal, E.; Hess, B.; van Buuren, A. R.; Apol, E.; Meulenhoff, P. J.; Tieleman, D. P.; Sijbers, A. L. T M.; Feenstra, K. A.; van Drunen, R.; Berendsen, H. J. C.; Gromacs User Manual, version 3.2, www.gromacs.org, **2004**.
(55) Berendsen, H. J. C.; van der Spoel, D.; van Drunen, R.; *Comput. Phys. Comm.* **1995**, 91, 43.
(56) Lindahl, E.; Hess, B.; van der Spoel, D.; *J. Mol. Mod.* **2001**, 7, 306.
(57) Yelena, A. Arnautova; Anna Jagielska, Harold A. Scheraga; *J. Phys. Chem. B* **2006,** 110, 5025
(58) Preliminary data have been recorded for the 20 naturally occurring amino acids as well as for allothreonine and homoserine; Myung, S.; Julian, R. R.; Clemmer, D. E. (work in progress).

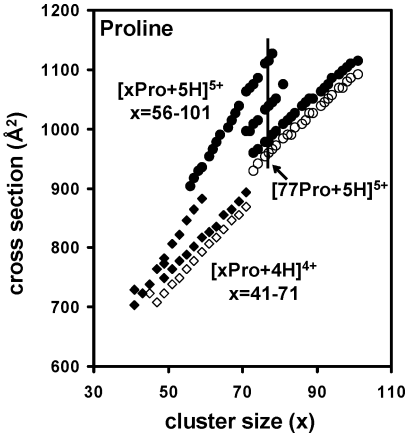

Figure 3. Experimental collision cross sections (Å^2) obtained for [xPro + 4H]$^{4+}$ (diamond, $x = 41-71$), and [xPro + 5H]$^{5+}$ (circle, $x = 56-101$) cluster ions. The solid and open symbols refer to cross sections obtained for enantiopure (100:0 L:D) and racemic (50:50 L:D) proline clusters, respectively. Note that several different cross section values are resolved from the $n = 4$ and 5 enantiopure clusters whereas only one structural family is observed from all racemic clusters. For example, three different cross section values are shown for enantiopure [77Pro + 5H]$^{5+}$ cluster ion (indicated by the vertical line) whereas the same racemic cluster size shows only one cross section. See text for more detail.

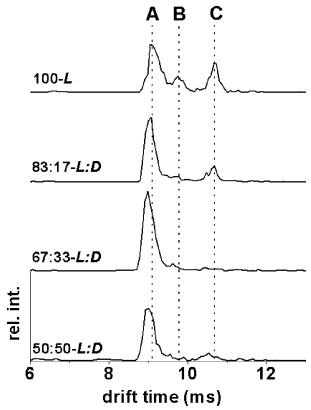

Figure 4. Drift-time distributions for [77Pro + 5H]$^{5+}$, obtained by integrating narrow regions of the two-dimensional IMS-MS datasets corresponding to: 100:0 L:D, 83:17 L:D, 67:33 L:D, and 50:50 L:D ratios of electrosprayed proline solutions. Positions of three maximum peaks are denoted by dashed lines A, B, and C, in the order from spherical to elongated structures based on their collision cross section as shown in Figure 3. The elongated structures are only observed from the enantiopure (100:0 L:D) solution whereas a single compact peak is observed from the racemic (50:50 L:D) solution. See text for more detail.

The two resolved peaks indicate that two stable families of conformations that do not interconvert during the experimental time scales must be present. The lower mobility (larger collision cross section) family is the only state observed for the small [41Pro + 4H]$^{4+}$ to [47Pro + 4H]$^{4+}$ sizes, and this family persists to [59Pro + 4H]$^{4+}$. The abundance of higher mobility (more compact) peak (A) is first observed for [48Pro + H]$^{4+}$ and increases in abundance with increasing cluster size, eventually becoming more abundant than the lower mobility species (B). The broad nature of peak (A) is evidence for multiple structures with similar collision cross sections that are not fully resolved under the conditions employed.

Similarly, several ion mobility distributions corresponding to [xPro + 5H]$^{5+}$ ($x = 63$, 72, 76, and 78) are also shown in Figure 2. A narrow peak (C) arriving at 9.05 ms is observed for [63Pro + 5H]$^{5+}$. As the cluster size increases for the $n = 5$ charge-state family, three peaks are measured (starting at $x = 73$ and persists to $x = 78$). These data require that at least three different structures coexist. These higher mobility peaks are labeled (A) and (B). Similar to peak (A) in $n = 4$ charge-state family, peaks (A) and (B) in $n = 5$ family are relatively broad, indicating that more unresolved structures within these regions exist. The relative abundances of peaks (A) and (B) increase with cluster size. As observed from Figure 2, peak (A) dominates the distribution for [78Pro + 5H]$^{5+}$. The additional lower mobility peaks observed for $n = 4$ and 5 charge states from enantiopure proline solution contribute a small but significant fraction of the total ion intensity, about 5%.

Summary of Experimental Cross Sections and Structural Families. Figure 3 shows the summary of cross sections determined by using the collision cross section equation for uniquely identifiable proline clusters in the $n = 4$ and 5 charge-state families. The solid and open symbols refer to enantiopure (100:0 L:D) and racemic (50:50 L:D) proline clusters, respectively. As described above, several structures (forming distinct slopes in Figure 3) are resolved for a single enantiopure cluster size, whereas only one structural family is observed for the racemic proline clusters for each n. A prominent feature in Figure 3 is the significant difference between the enantiopure (solid symbols) and the racemic (open symbols) clusters for the larger clusters where cross sections may differ by more than 10% (e.g., the range associated with the [77Pro + 5H]$^{5+}$ ion).

Variations with Enantiomeric Excess. The analysis of the drift-time distributions obtained for individual clusters as a function of enantiomeric excess reveals interesting clues about the influence of chirality on cluster formation. Figure 4 shows drift-time distributions for the [77Pro + 5H]$^{5+}$ when formed from solutions containing 50:50, 67:33, 83:17, and 100:0 L:D compositions. Data recorded (not shown in Figure 4) for 33:67, 17:83, and 0:100 L:D solution compositions are indistinguishable from their counterparts 67:33, 83:17, and 100:0 L:D solutions, respectively. In this cluster, we observe three mobility peaks. The lower mobility peaks (larger collision cross section) (B) and (C) are only observed from the enantiopure (100 L) solution while a single higher mobility peak (A) is observed for the racemic (50:50 L:D) solution. Comparison of experimental cross sections with values calculated for model geometries generated from the crystal structures of enantiopure and racemic proline[51,52] (over 50−100 size range) indicates that peak (A) corresponds roughly to spherical structures, whereas peaks (B) and (C) correspond to ions with more elongated geometries. Extended structures (any structures other than random aggregates, which should have spherical structures) are only expected if the constituent proline molecules are well organized. These data (and similar results for other sizes) show that the abundance of the elongated geometries depends strongly on the chiral composition of the solution from which the clusters are electrosprayed. Therefore, these geometries are favored from solutions that are enriched in one chiral form (most abundant from enantiopure solutions) and appear inhibited when the other enantiomer is added. That is, over this size regime for proline, enantiopurity favors structural organization whereas chiral heterogeneity does not.

Molecular Models. Constructing a molecular model for the proline clusters that will provide insight into the relationship between cluster structure and thermodynamic stability as a

Table 1. Cross Sections and Formation Energies for Pro_{68} Clusters

structure	Ω_{expt} (Å^2)[b]	Ω_{calc} (Å^2)[a,e]	ratio expt/calc[e]	Ω_{calc} (Å^2)[a,f]	ratio expt/calc[f]	ΔE(kcal·mol^{-1})[f,g,h]
enantiopure Pro_{68}(sphere)	872[c]	916	0.952	867	1.006	−2379
enantiopure Pro_{68}(rod)[i]	1027[d]	1019	1.008	1012	1.015	−2139
racemic Pro_{68}(sphere)	853[c]	889	0.960	874	0.976	−2275
racemic Pro_{68}(rod)[i]		1021		1013		−1822

[a] Calculated using the exact hard spheres scattering method.[53] [b] Experimental results. [c] Cross section obtained for $[68Pro + 4H]^{4+}$. [d] Cross section obtained for $[68Pro + 5H]^{5+}$. [e] Unminimized trial structures. [f] Minimized trial structures. [g] Formation energies. [h] The Lennard-Jones (LJ) parameters are $\epsilon = -0.47$ kcal·mol^{-1} and $\sigma = 0.277$ nm. [i] The ratio of length to diameter is 2:1.

function of enantiopurity is challenging. The use of routinely available force fields that are primarily designed to simulate proline in proteins is expected[57] and confirmed here to lead to instabilities and structural collapse in classical molecular mechanics simulations. More carefully constructed models should yield substantial benefits. Because of this, we invested significant efforts in deriving a more specialized set of force field parameters. Details of the force field generation process are given in the Supporting Information. In short, the interactions governing the overall structure and energy of the clusters are divided into two parts, the *intra*molecular V_{intra} and *inter*molecular V_{inter} potentials. The former contains bond stretch and angle/dihedral distortion energies, whereas the latter is dominated by Coulombic and Lennard-Jones (LJ)-type nonbonded interactions. We utilized density functional quantum calculations on a proline monomer at the B3LYP/cc-pVTZ(-f) level of theory,[59,60] as implemented in the Jaguar package,[61] to determine V_{intra} and the atomic charges for Coulombic force calculations. The LJ potentials were optimized iteratively within the new set of parameters as to best reproduce experimentally observed density of L- and LD-proline crystals.[51,52]

First, trial geometries for large clusters were generated from the crystal structures of L- and LD-proline.[51,52] Similar to our previous work on serine,[29] different sizes and geometries were used initially without further structural refinement to gain insight to the overall shape of the large proline clusters. These initial studies suggested that higher-mobility families of ions have roughly spherical geometries,[29] whereas only enantiopure proline clusters contain additional structures that have experimental cross sections greater than a sphere by ∼4−12%. These preliminary unminimized structures were then refined using the new force fields for a cluster system containing 68 proline units, where spherical and rod-shaped geometries were considered for both enantiopure and racemic clusters. The optimized structures are shown in Figure 5. Note that there is no net charge.

To compare these structures with experiment, we calculate their collision cross sections as described above.[53] The results are summarized in Table 1. For unminimized structures, the cross sections for an enantiopure sphere geometry differs from the racemic sphere geometry by ∼3%. The cross sections calculated for an unminimized enantiopure rod geometry is nearly identical to a racemic rod structure, differing by only ∼0.2%. The differences between enantiopure and racemic cross sections for spherical geometries are reduced to <1% when structures are minimized. These cross section calculations show that structures contract slightly upon minimization for both the sphere and rod geometries. For example, cross sections for unminimized structures for the sphere and rod geometries of

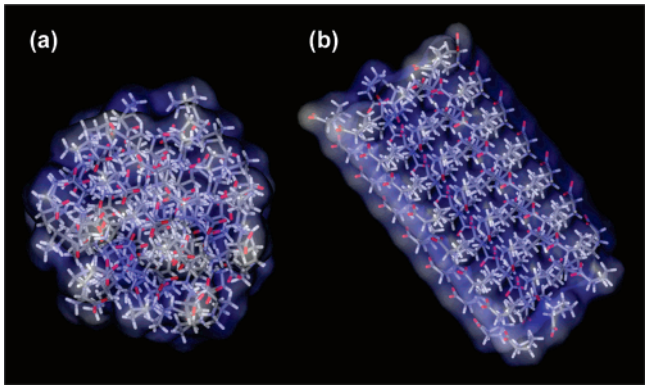

Figure 5. Optimized structures obtained for the (a) spherical and (b) rod-shaped L-Pro_{68} cluster size.

enantiopure Pro_{68} decrease by ∼5% (916−867 Å^2) and 1% (1019−1012 Å^2), respectively, upon minimization. Overall, comparisons in Table 1 show that there is good agreement between the cross sections for minimized geometries and experiment.

In general, comparing energies that are obtained in classical molecular mechanics calculations is problematic, as the underlying force field may not be able to give sufficiently consistent and accurate models. Here, we employ a carefully calibrated, customized force field (see Supporting Information for details), and the monomers are essentially rigid in structure, eliminating intramolecular energy changes as a potential source of serious error. Although the absolute energies obtained in our simulations are probably not accurate in a quantitative sense, we expect that the overall trends observed by comparing the computed energies are physically meaningful, especially when substantial energy differences are found. The calculated cluster formation energies are also listed in Table 1. Spherical clusters are most stable with total energies of −2379 and −2275 kcal·mol^{-1} for the enantiopure and racemic clusters, respectively. These energies can be normalized to average interaction energies of −35.0 and −33.5 kcal·mol^{-1} per proline molecule in the cluster. The rod-shaped geometry is energetically disfavored with cluster formation energies of −2139 and −1822 kcal·mol^{-1} for the enantiopure and racemic samples, respectively, giving rise to averaged interaction energies of −31.5 and −26.8 kcal·mol^{-1} per molecule. Thus, the rod-shaped Pro_{68} cluster is 240 kcal·mol^{-1} higher in energy than the spherical cluster when the enantiopure sample is used. In the case of the racemic sample, the energetic penalty for forming the rod-shaped cluster nearly doubles, increasing to 453 kcal·mol^{-1}. That is, from an energetic standpoint, structural variation away from the most stable spherical shape is substantially more costly for the racemic sample than for the enantiopure sample.

The underlying cause of this difference is easy to understand. Upon examining theoretical structures, we find that in the

(59) Becke, A. D. *J. Chem. Phys.* **1993**, 98, 5648
(60) Lee, C. T.; Yang, W. T.; Parr, R. G. *Phys. Rev. B.* **1988**, 37, 785
(61) Jaguar 5.5, Schrödinger, L. L. C., Portland, OR **1991**−**2003**.

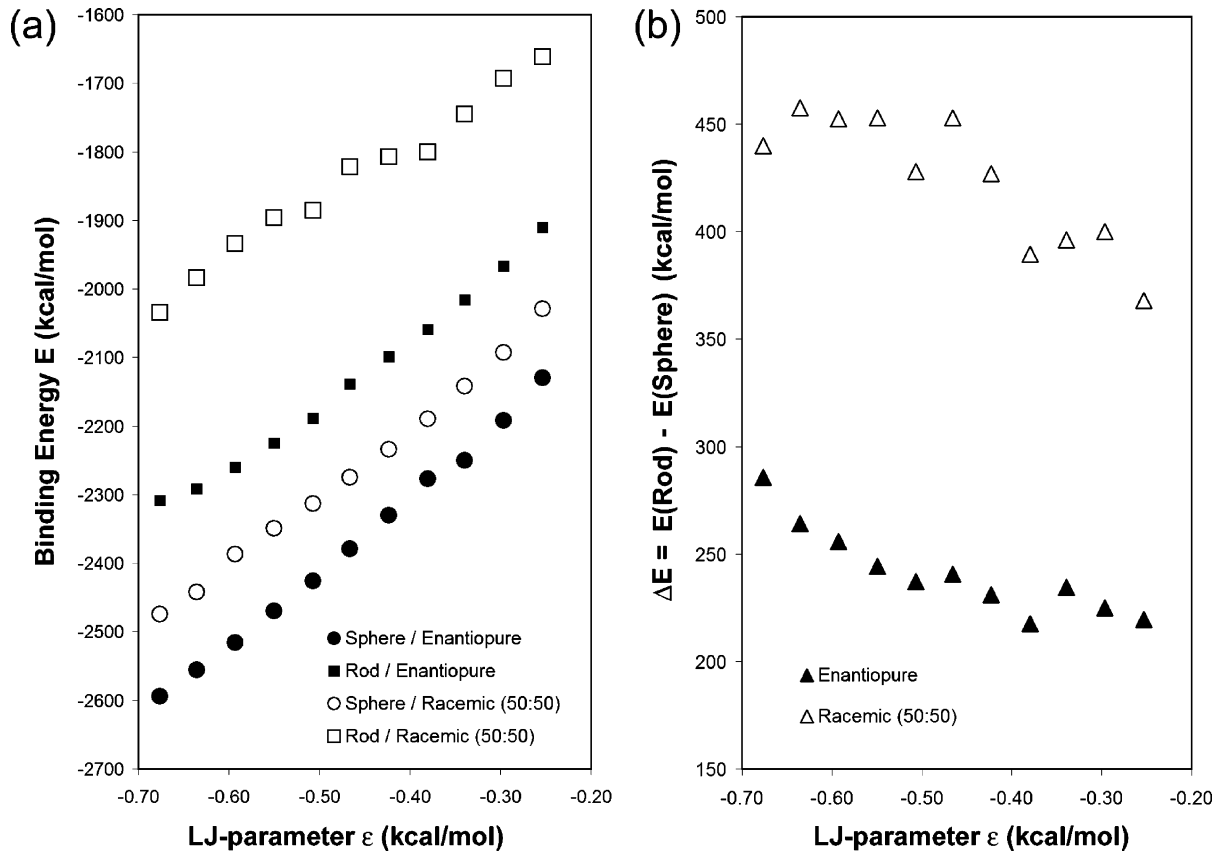

Figure 6. Plots of (a) computed binding energy (kcal·mol^{-1}) as a function of Lennard-Jones (LJ) parameter ϵ (kcal·mol^{-1}) and (b) energy differences as a function of the LJ potential parameter ϵ (kcal·mol^{-1}) obtained for Pro_{68} cluster size. The solid and open symbols refer to the enantiopure and racemic clusters, respectively. The different trial geometries are denoted by square (rod) and circle (sphere). As shown in (a), the binding energy becomes more stable (indicated by more negative values) as ϵ becomes more negative. To the right, the energy differences increase as proline−proline interactions become stronger (indicated by more negative values of ϵ). See text for detailed description on the influence of these energetics in the formation of specific structures.

enantiopure ensemble, the alignment of the proline units is more uniform, resulting in strong proline-proline interactions. If a 50:50 mixture of L:D-proline is used, the monomer units are relatively mismatched, giving rise to partial loss of the favorable proline−proline interactions. Ultimately, these clusters are less stable. In rod-shaped geometries, more molecules are placed on the surface, reducing the total number of the favorable proline−proline interactions. When this occurs for enantiopure clusters, the proline molecules are still better aligned than in the racemic clusters. Thus, the energetic penalty for the enantiopure clusters is reduced because the monomer units maintain a network of matched proline-proline interactions. Assuming perfect mixing, this model indicates that the energy difference between the racemic and enantiopure clusters in the rod-shaped geometry is 317 kcal·mol^{-1}, which correlates to an average energy difference of 4.7 kcal·mol^{-1} per molecule.

Although these considerations provide a semiquantitative explanation that is consistent with the experimental findings, and begins to explain why the energetically unfavorable rod-shaped geometry is more accessible for the enantiopure sample than for the racemic samples, we were somewhat surprised by the magnitude of the computed energy differences. To understand the underlying principle in more detail, we conducted a computational experiment wherein the long-range LJ potential parameter ϵ (which was determined to be −0.47 kcal·mol^{-1} to reproduce the packing density of the experimental crystal structure) was both increased and decreased with respect to the crystal structures of L- and LD-prolines.[51,52] Figure 6 shows the results of these studies. The overall stability of all clusters increases when the proline−proline interactions become more attractive, as indicated by more negative cluster formation energies when ϵ becomes more negative (Figure 6a). More interestingly, these calculations suggest that the energy difference between the spherical and rod-shaped geometries is sensitive to the proline−proline interaction strength (Figure 6b). For both the enantiopure and racemic samples, the energy differences between spherical and rod-shaped structures increases as the proline−proline interactions become stronger. Note that the energy fluctuations (i.e., scatter in the data, which are directly correlated to increase of misalignment) are significantly higher in the racemic cluster as the LJ-parameter is varied (Figure 6b, empty triangles). The overall trend, however, is that the energy differences increase as the LJ-parameter, ϵ, becomes more negative.

This conceptual understanding can be tested by experiment. Figure 7 shows cross section distributions for clusters of *cis*-4-hydroxy-proline. The additional OH group should significantly increase the intermolecular forces by explicit hydrogen-bonding interactions. From our semiquantitative understanding, we would predict that increasing the intermolecular interactions will increase the energetic preference for the spherical cluster shape. This is certainly the experimental case. For the equivalent n = 4 and 5 clusters, we observed only single peaks in the IMS-MS data. There are no significant differences in cross section between the enantiopure and racemic clusters of *cis*-4-hydroxy-proline. Moreover, the plot (Figure 7) of cross section versus

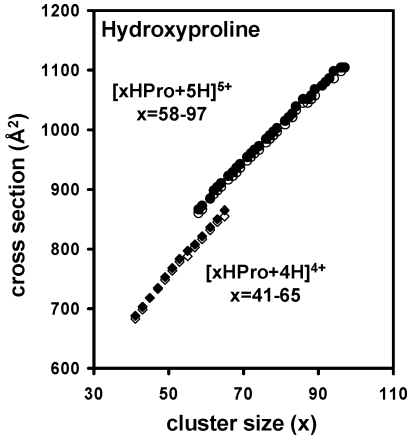

Figure 7. Experimental collision cross sections (Å^2) obtained for [*x*HPro + 4H]$^{4+}$ (diamond, $x = 41-65$), and [*x*HPro + 5H]$^{5+}$ (circle, $x = 58-97$) cluster ions. The solid and open symbols refer to the experimental collision cross sections derived from enantiopure (100:0 L:D) and racemic (50:50 L:D) *cis*-4-hydroxy-proline clusters, respectively. Note that only a single family of spherical geometries is observed for all clusters.

cluster size shows that clusters grow in a systematic fashion, indicating that clusters of different sizes have similar shapes. And, in this case, they are roughly spherical.

Summary and Conclusions

IMS-MS and molecular modeling techniques were employed to investigate proline and *cis*-4-hydroxy-proline clusters in the gas phase. Several families of structures are observed: a family of compact structures from the racemic proline and *cis*-4-hydroxy-proline clusters and three structures (ranging from spheres to rodlike) for the enantiopure proline clusters. These geometries do not interconvert over the 15−20 ms experimental time scale. Classical molecular mechanics simulations utilizing force fields that were specifically optimized suggest that the higher mobility ions correspond to spherical aggregates whereas the extended structures are elongated structures that can be approximated conceptually as rod-shaped clusters. Taken together, our experimental and computational studies indicate that chirality has a significant impact on the formation of the elongated structures where they are only formed from an enantiopure solution. Two conclusions about the organized assembly of chiral structures can be drawn. First, the chiral center must be emphasized through some type of structural or functional mechanism.[62] In the case of proline, the rigidity and the hydrophobicity of the cyclic side chain serves to emphasize the importance of the chiral center during noncovalent cluster formation processes. Second, enantiopurity must be present to further facilitate structural organization in a system that meets the first condition. Both factors are accounted for within the enantiopure proline clusters, thus allowing this system to display measurable assembly of large chirally organized structures.

The combination of experiments and computations provides an insight into the finely tuned balance between the intermolecular attraction, structural alignment, and overall accessibility of different cluster geometries. The conceptual model that emerged from our study may be fundamental to other assembly processes.

Acknowledgment. This work is supported in part by grants from the National Science Foundation (CHE-0078737 and 0116050), National Institute of Health (HG003894) and Indiana University METACyt initiative funded from the Lilly Endowment.

Supporting Information Available: Complete description of the computational details, Cartesian coordinates of all structures and all energy components. In addition, the full list of authors in ref 42b. This material is available free of charge via the Internet at http://pubs.acs.org.

JA0622711

(62) Klussmann, M.; Iwamura, H.; Mathew, S. P.; Wells, Jr. D. H.; Pandya, U.; Armstrong, A.; Blackmond, D. G. *Nature* **2006**, 441, 621.